

# Proton-rich and neutron-rich hypernuclear production experimental conditions

C. Rappold<sup>1,2,\*</sup> and J. F. López Fidalgo<sup>2</sup>

<sup>1</sup>*GSI Helmholtz Centre for Heavy Ion Research, Planckstrasse 1, 64291 Darmstadt, Germany*

<sup>2</sup>*Universidad Castilla-La Mancha, Institute of Mathematics applied to Science & Engineering, Avenida Camillo José Cela 3, 13071 Ciudad Real, Spain*

(Dated: December 3, 2024)

After the demonstration of the feasibility of hypernuclear spectroscopy with heavy-ion beams by the HypHI collaboration, the study of proton- and neutron-rich hypernuclei is the next phase that the HypHI collaboration focuses on. The use of the fragment separator for the production of rare isotope beam is a crucial aspect to produce hypernucleus far from the stability line. Precise spectroscopy of exotic hypernuclei is planned to be carried at GSI and later at FAIR facility with the FRS and Super-FRS separators. A systematic study and optimization analysis were performed in order to determine the optimal experimental conditions for producing hypernuclei with high isospin. The optimal conditions are obtained based on theoretical models for the heavy-ion induced reaction hypernuclear production and Monte Carlo simulations of the Fragment separator in order to include experimental efficiencies for the production of exotic secondary beam. The developed methodology is presented to deduce the expected yields of  ${}^8_{\Lambda}\text{Be}$  while other proton-rich and neutron-rich hypernuclei are also estimated afterwards.

PACS numbers: 21.80.+a, 25.60.-t, 25.70.Mn

## I. INTRODUCTION

The interest in strangeness production in nuclear and hadron collisions has been growing during the last decades. From the standard nuclear matter composed by ordinary nucleons, formed by triplets of the two lightest d- and u-quarks, the strange (s) quark is necessary to be considered in order to understand the properties of the dense matter [1, 2]. It has been demonstrated that a bound system of nucleons and hyperons (baryon including at least one s-quark) can be a key feature to study those hyperon-nucleon and hyperon-hyperon interactions [3]. The bound system of nucleons and hyperons is called a hypernucleus. At GSI Helmholtz Centre for Heavy Ion Research, Darmstadt (Germany) a new activity on the topic of hypernucleus has been carried on since 2006 [4]. First experiments took place in the GSI accelerator facility. They aimed and succeeded to demonstrate the feasibility of performing a precise spectroscopy of hypernuclei produced in heavy-ion induced reactions [5–7], thanks to a novel experimental method differing from the established methodology [8]. In addition a possible new bound state has been found: the association of two neutrons and  $\Lambda^0$  hyperon, forming a possible neutral nucleus [6]. New experiments are considered to be performed in the fragment separator, FRS [9–11], of GSI in order to either confirm or deny the existence of such a bound state.

The first experiment of the HypHI collaboration aimed to demonstrate the feasibility of the hypernuclear spectroscopy by means of heavy ion beam induced reactions. The Phase 0 experiment was performed with a  ${}^6\text{Li}$  beam at 2 AGeV impinging on a stable  ${}^{12}\text{C}$  target material.

The main goal of the experiment was to produce, reconstruct and identify decay vertexes of  $\Lambda$  particle and  ${}^3_{\Lambda}\text{H}$ ,  ${}^4_{\Lambda}\text{H}$  and  ${}^5_{\Lambda}\text{He}$  hypernuclei [4]. With the finalized data analysis of Phase 0 experiment, the final results show that the experimental method is viable for the study of hypernuclei [5]. A second experiment with a  ${}^{20}\text{Ne}$  beam with the similar condition was also performed, and its data analysis is ongoing.

The future phases of the project focus on the study of exotic hypernuclei which can not be produced in typical missing mass experiments involved at JPARC, JLab or MamiC [4]. The study of exotic hypernuclei toward the proton- and neutron-drip line necessarily involves the use of rare-isotope beams. One of the main goals of the HypHI project is to extend the hypernuclear chart to the proton drip line up to  $\Lambda\text{Si}$  hypernuclei and neutron drip line up to  $\Lambda\text{Li}$  hypernuclei. A larger charge symmetric breaking effect may be expected in proton- and neutron-rich hypernuclei. It may cause a change in the difference between  $\Lambda$ -proton and  $\Lambda$ -neutron interactions which may induce a shift of the drip-line positions.

The HypHI project carries on its second phase, in which the study of proton-rich hypernuclei will be performed. For this purpose a new experimental concept has been in development. The Super-FRS fragment separator is crucial to the future phases of the HypHI project at FAIR. A feasibility study of the Super-FRS capability toward high energy of around 2.0 AGeV had to be achieved. The study reported in this article aimed at determining which experimental conditions are necessary for the production of proton-rich or neutron-rich hypernucleus. The primary beam and target isotopes have to be chosen to obtain the exotic beam of interest at 2 AGeV which will then be bombarded on the secondary production target to produce the subsequent exotic hypernucleus of interest. First, the different models and

---

\* c.rappold@gsi.de

simulations used for this purpose will be presented. It is then followed by the method developed for combining all those information into a multivariate dataset which allows to extract the optimal experimental conditions for any possible hypernucleus of interest.

## II. SIMULATION PROCESSES

The systematic study and the development of optimization processes try to propose a data-processing based method to find and decide what can be the optimal experimental conditions for the production of a specific exotic hypernuclei. In the first experiment of the HyPHI collaboration the experimental apparatus was based on an open geometry in which any produced hypernuclei within the projectile rapidity region could be measured inclusively. In the next phase of the project, within the FRS and Super-FRS fragment separator, the experimental apparatus will focus on exclusive measurement of a specific hypernucleus since the fragment separator will be set for a specific momentum range or magnetic rigidity. It will allow a more precise invariant mass measurement of the reconstructed hypernucleus thanks to a better momentum resolution of the FRS and Super-FRS. Therefore, the fragment separator setting or experimental conditions have to be determined beforehand. Especially, which exotic secondary beam has to be produced and used on a secondary target for the production of the desired hypernucleus.

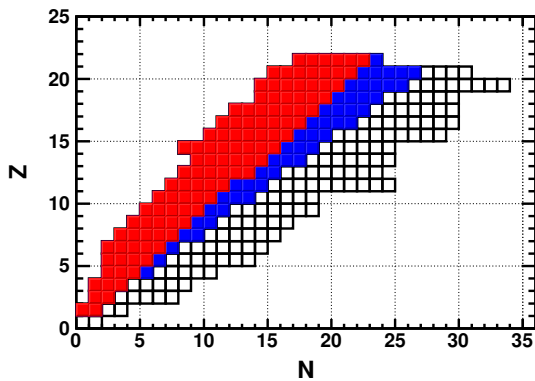


FIG. 1. (Color online) The nuclear chart, neutron ( $N$ ) versus proton number ( $Z$ ), of the exotic isotopes that was obtained in the EPAX calculations through nuclear collisions up to  $^{40}\text{Ca}$ - $^{40}\text{Ca}$ . The isotopes which have a magnetic rigidity at 2AGeV accepted within the FRS and SuperFRS are shown in red and blue color respectively.

A first systematic study based EPAX [12, 13] theoretical model was performed. The EPAX calculation provides the production cross section of exotic or normal nuclei for the collision of a given stable beam and target species. EPAX model is based on an empirical parametrization of the fragmentation cross sections

[12, 13]. Large samples of beam-target combination were produced as an initial database for the Monte Carlo simulations of the fragment separator. Those calculations are used to determine the normalized yield per centimeter of target. The comparison between the different beam-target combinations is then used to preselect the most interesting beam-target combination. All possible exotic isotopes from Hydrogen to Scandium have been calculated from all possible combination of stable isotopes up to  $^{40}\text{Ca}$  Calcium. Fig. 1 shows the chart of the isotopes whose cross section have been calculated by the EPAX model. At 2AGeV only a restricted number of isotopes are usable within the FRS and SuperFRS because of their maximum acceptable magnetic rigidity; 18 Tm and 20 Tm respectively. Those isotopes are shown in red and blue color respectively in Fig. 1.

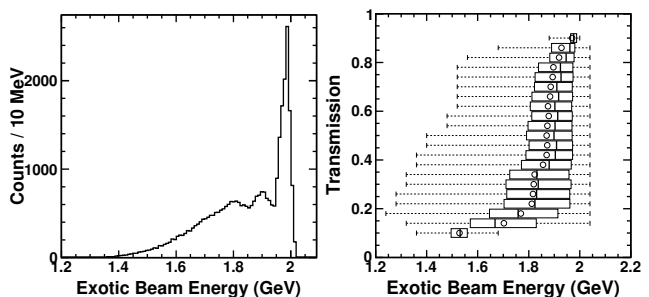


FIG. 2. Kinetic beam energy distribution and transmission distribution of the fragments propagated by MOCADI simulations. The projected beam energy distribution is shown on the left panel. The candle plot of beam energy distribution as a function of the transmission is shown on the right panel. For each transmission bin, the box represent the underlying distributions: The bold line represent the quantile at 50%, the left and right side of the box are the 75% and 25% quantile. The maximum and the minimum of the distributions are represented by the vertical segments of the dotted line. The open circle is the position of the mean value of distributions.

Afterward, the obtained database of the possible exotic isotopes is used in the MOCADI Monte Carlo simulations [14]. Those MOCADI Monte Carlo simulations were employed for calculating the transmission and yield of each possible exotic secondary beam of the database within the Super-FRS. The secondary beam of interest and exotic isotopes which have a similar magnetic rigidity to the one of the exotic beam are transported from the production target location up to the FMF2 experimental area of the SuperFRS [15, 16]. In the FMF2 experimental area, a secondary production target will be placed for the hypernuclear production. The systematic study is then extended to include the secondary beam yield from all the possible set of beam and target species at several target thicknesses. It was simulated as such to find the optimal parameters for obtaining the highest intensity of the secondary beam of interest at FMF2 of the Super-FRS. More than thirty  $5 \times 10^3$  MOCADI setup were run

in which each the MOCADI simulations were optimized over 6 runs of  $10^4$  events to obtained the best transmission of the secondary beam of interests. Results from the MOCADI simulations are shown in Fig. 2, the resulting distribution of the kinetic energy of fragment beam and the kinetic energy as a function of the transmission between the production target and the FMF2 area. For the optimal conditions for a secondary beam will be a beam energy as close as possible to 2 AGeV for maximizing the hyperon production with a reasonable transmission to the FMF2 experimental area.

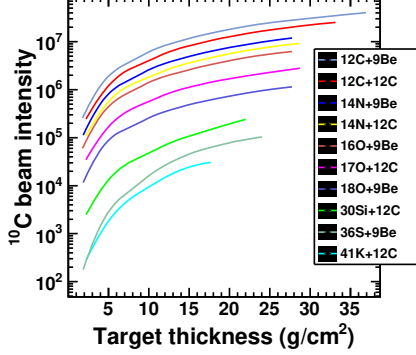


FIG. 3. (Color online) Intensity of secondary beam  $^{10}\text{C}$  at FMF2 experimental area of the SuperFRS as function of the production target density, the primary beam and target isotope. Only ten entries of results of MOCADI simulations are displayed out of all entries of the dataset. The intensity of the primary beam was set to  $5 \times 10^9$  per second, which will be available at the SuperFRS. The legend is ordered from highest to lowest intensity.

Fig. 3 shows a summary of case study for the production  $^{10}\text{C}$  secondary beam with a small sample of different primary beam/production target combination represented as a function of the target thickness. The calculation shows the reaction between (C, N, O) beam isotopes and (Be, C) target isotopes gives the highest  $^{10}\text{C}$  beam intensity up to several million ion per second for a primary beam intensity of  $5 \times 10^9$  ions per second. Fig. 3 only shows the possible optimal case when only the target thickness is considered for the optimal search. However, other parameters such as the contamination of other produced exotic isotopes, the beam energy or the secondary reaction for the hypernuclear production have to be considered and a more advanced methodology, that will be presented afterward, was developed to find the optimal combination of the experimental parameters.

The study of the production of the exotic hypernuclei for each secondary beam of interest is achieved thanks to the following theoretical model [17]. It is an hybrid model between the transport model DCM-QGSM (Dubna Cascade Model - Quark-Gluon String Model), which simulates the collision between the beam and the target, and a statistical approach for the Fermi break up model to describe the de-excitation of spectators. Each

case study of the hypernuclear production in the nucleus-nucleus collision at 2 AGeV are simulated with  $5 \times 10^7$  events. The theoretical calculation of the hypernuclear production cross section for  $^6\text{Li}+^{12}\text{C}$  collisions at 2 AGeV was performed as well in order to compare the published experimental results [7] to the model predictions. The theoretical results were compatible with the experiment, which give confidence into the other collisions calculations. Overall, more than  $3 \times 10^9$  events were simulated to construct a dataset of produced hypernuclei by exotic beam, from Li to Ne isotopes, colliding on a  $^{12}\text{C}$  Carbon or  $^9\text{Be}$  Beryllium target. The database can be ordered by colliding isotopes or by produced hypernuclei. Fig. 4 shows the hypernuclear production cross section in  $\mu\text{b}$  as function of the neutron and proton number of  $\Lambda$ -hypernuclei for a proton-rich  $^9\text{C}$  and neutron-rich  $^{15}\text{C}$  secondary beam on a  $^{12}\text{C}$  target. A clear difference can be seen with the case of the  $^{12}\text{C}+^{12}\text{C}$  collision, where the exotic carbon beam enhances exotic hypernuclear production between 1.2 to 3 times. In the case of the production of neutron-rich hypernuclei, higher increase is observed in the  $^{12}\text{B}$  exotic beam compared to the  $^{12}\text{C}$  beam case as shown in the Fig. 4. Opting the proton-rich exotic beam clearly favor the production of proton-rich hypernuclei, and reciprocally for neutron-rich hypernuclei.

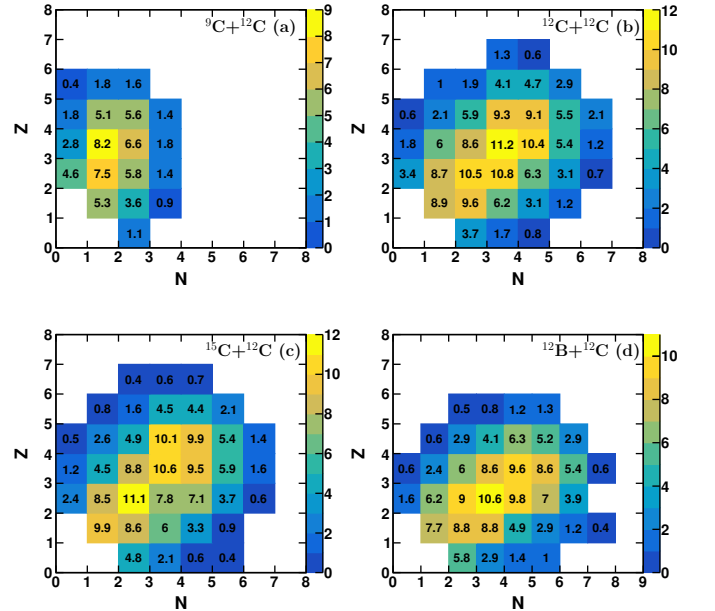


FIG. 4. (Color online) Production cross section in  $\mu\text{b}$  of hypernuclei from the collision 2AGeV of  $^9\text{C}+^{12}\text{C}$  (a) and  $^{12}\text{C}+^{12}\text{C}$  (b),  $^{15}\text{C}+^{12}\text{C}$  (c) and  $^{12}\text{B}+^{12}\text{C}$  (d) panel respectively.

When the database is ordered by produced hypernuclei, Fig. 5 shows the production cross section of proton-rich hypernucleus  $^8_\Lambda\text{Be}$  and neutron-rich hypernuclei  $^{11}_\Lambda\text{Be}$  at 2AGeV as a function of the neutron and proton number of the exotic beam reacting on a  $^{12}\text{C}$  target. The sec-

ondary beam isotope that maximizes the production of each exotic hypernucleus can be then determined. However, this maximum is not necessarily the optimal since the production of the exotic beam has to be also considered. When the kinetic energy of exotic beam varies from the 2 AGeV case, the hypernuclear production cross sections are scaled by the parametrization [18] used to fit the world data set of total production cross section of  $pp \rightarrow pK^+\Lambda$  [19]. The parametrization parameters used are from [19]. The function is then normalized by the value at 2 AGeV. For instance, the hypernuclear production cross section is then reduced by 73% or 46% if the energy of exotic beam is down to 1.9 AGeV or 1.8 AGeV respectively.

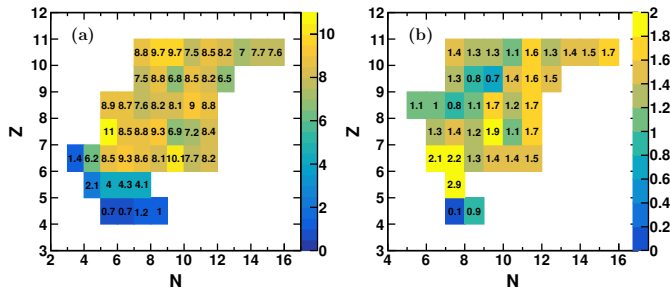


FIG. 5. (Color online) Production cross section in  $\mu\text{b}$  of  ${}^8_\Lambda\text{Be}$  and  ${}^{11}_\Lambda\text{H}$  hypernucleus from collision of different exotic secondary beam  ${}^{Z+N}\text{Z}$  on a  ${}^{12}\text{C}$  at 2 AGeV (a) and (b) panel respectively.

A multivariate dataset was then created in which the results of those theoretical calculations and Monte Carlo simulations are gathered in order to find the optimal set of experimental parameters to maximize the production of a hypernucleus of interest. This parameter set includes which primary beam, which production target, and which exotic secondary beam are best to produce the hypernucleus of interest. Additionally it includes which thickness of the production target and the amount of parasitic secondary beams are also produced for a specific pair of primary beam and production target species. A generic methodology was developed independently of the hypernucleus of interest so that it can be applied to any interested hypernucleus to determine the most optimal experimental setup for its study.

### III. MULTIVARIATE ANALYSIS

It is merely impossible to simply plot the multivariate dataset and estimate which can be the best case by compiling all the possible combinations and permutations of the isotopes species. An optimization procedure had to be used to find this optimal case. In the article we focus first on the production of the proton-rich hypernucleus  ${}^8_\Lambda\text{Be}$ , yet other hypernuclei are considered afterward

since the optimization procedure does not depend of the hypernuclear species.

In an optimization problem, a cost function has to be defined between the different parameters in order to find the optimal set which maximize or minimize this cost function. The cost function was defined as such for our multivariate dataset:

$$F(Cs, E, Th, In) = \alpha \cdot Cs + \beta \cdot E - \sqrt{1 - \alpha^2 - \beta^2} \cdot Th + 1/2 \cdot In \quad (1)$$

in which  $Cs$ ,  $E$ ,  $Th$ ,  $In$  refer to the hypernuclear yield, the secondary beam energy, the production target thickness, and the intensity of the secondary beam of interest respectively. The parameters  $\alpha$  and  $\beta$  defined in the cost function  $F$  are the weight coefficients that connect the different variables. In the cost function, the different parameters space has been normalized to be within  $[0,1]$  interval in order to keep the weight coefficients within the unit interval. The coefficient  $\alpha$  and  $\beta$  are set arbitrary depending how much weight is considered to be associated to each dataset parameters. This cost function is built intentionally to maximize the production of the hypernucleus of interest, like  ${}^8_\Lambda\text{Be}$  in our case study by obtaining an optimal intensity of the secondary beam in which the thickness of the production target is minimized.

In this process the production of the hypernucleus of interest is taken into account. From the theoretical calculations of the hypernuclear production all possible secondary beam on Beryllium or Carbon target are considered. The secondary beam selected by the procedure is used to find the optimal conditions of the Super-FRS, then the hypernuclear yield per second is calculated for a 4-centimeter secondary production target. The simple case of using stable beams for the hypernuclear production is also included in the dataset. An intensity a  $10^7$  ion per second was selected in those cases of stable beam to estimate the hypernuclear yield per second.

A search for the cost function's maximum is then performed to determine the optimal parameter set for a fixed  $\alpha$ - $\beta$  pair. One can also investigate the evolution of what is the optimal variables obtained as a function of those weight coefficients. Fig. 6 shows the different results of the optimization as a function of  $\alpha$  and  $\beta$  weight parameters. First in (a) panel of Fig. 6, the distribution of the cost function maximum as a function of  $\alpha$  and  $\beta$  is presented. Each value of this distribution is a possible optimal condition set, yet a maximax criterion was selected in order to decide which are the best optimal condition that we should consider. In the (b)-(g) following panels of Fig. 6, the evolutions of the variable set of database as a function of  $\alpha$  and  $\beta$  are presented. The optimal isotope species of the primary beam and target are shown in panel (b) and (c), while the target thickness in centimeter in panel (d). The secondary beam that should be selected for the optimal production of  ${}^8_\Lambda\text{Be}$  and its resulting kinetic energy for each  $(\alpha, \beta)$  is shown in panel



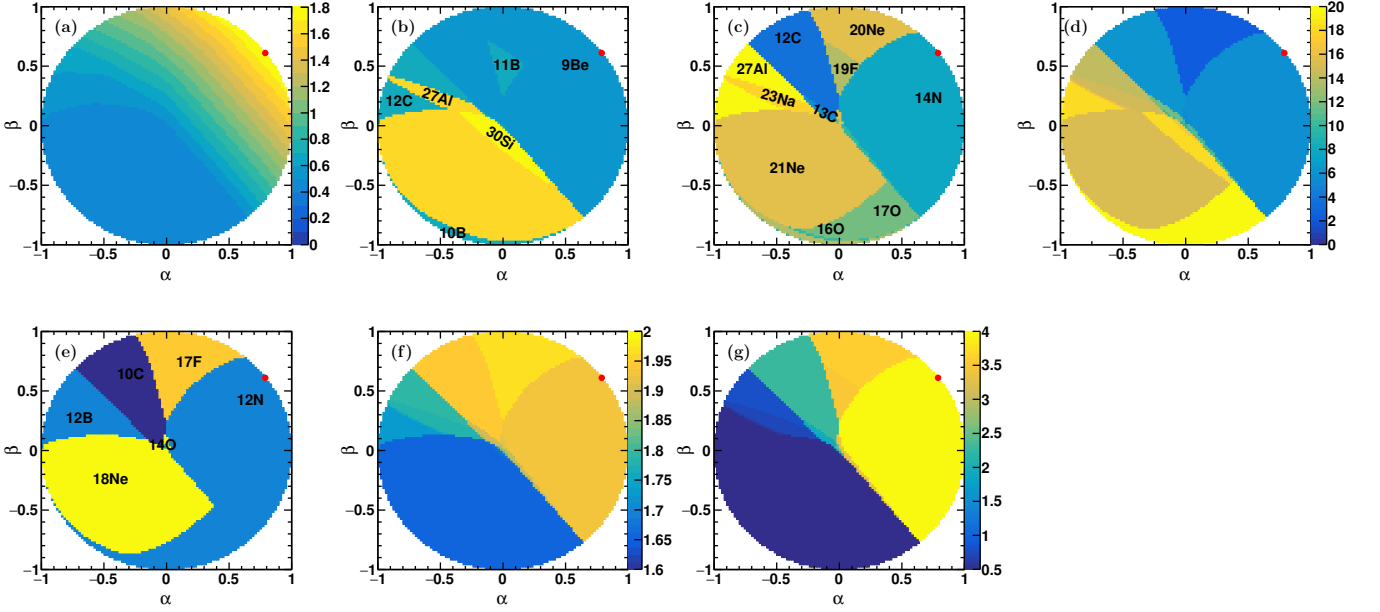


FIG. 6. (Color online) Results of the multivariate dataset optimization for the study case of  ${}^8_{\Lambda}\text{Be}$  as a function of the primary beam and target species, the target thickness, the exotic beam species. Panel (a) shows the evolution of the cost function maximum as a function of the  $\alpha$  and  $\beta$  weight parameters, while panel (b) to (g) represent the evolution of the variables, the target and primary beam species, the thickness in centimeter, the selected exotic beam species and its kinetic energy in AGeV, and  ${}^8_{\Lambda}\text{Be}$  yield per second respectively. The red circle shown in all panels represents the position of the overall maximum within the  $\alpha$ - $\beta$  search.

(e) and (f) respectively. The yield per second of  ${}^8_{\Lambda}\text{Be}$ , produced by the collision of the optimal secondary beam and a 4-centimeter  ${}^{12}\text{C}$  target, is finally shown in panel (g) as a function of  $\alpha$  and  $\beta$ . The evolution of the weight parameters  $\alpha$  and  $\beta$  between  $[-1, 1]$  represents the intention of minimizing or maximizing the influence of the variables  $C_s$  and  $E$  in the cost function. For instance, when  $\alpha$  is negative the overall intention is to minimize the hypernuclear yield or when  $\beta$  is negative the intent is to minimize the kinetic energy of the optimal secondary beam. It is useful to calculate the optimal conditions within the  $[-1, 1]$  weight parameters interval since another decision criterion can be considered instead of the maximax approach.

In the case of  ${}^8_{\Lambda}\text{Be}$ , shown in Fig. 6, the systematic procedure gives the following set of experimental parameters: with a primary beam of  ${}^{14}\text{N}$  on a production target of  ${}^9\text{Be}$  with a thickness of 5.5 centimeters, an exotic beam of  ${}^{12}\text{N}$  should be selected and bombarded a  ${}^{12}\text{C}$  target. The intensity of  ${}^{12}\text{N}$  secondary beam is about  $5.1 \times 10^6$  ions per second with a primary beam of  $5 \times 10^9$  ions per second, which is within the expected intensity that the new FAIR facility will provide at the entrance of the Super-FRS. Subsequently, the  ${}^8_{\Lambda}\text{Be}$  counting rate under those conditions is about 4.0 produced hypernuclei per second for a 4-centimeter secondary target.

After showing the details for  ${}^8_{\Lambda}\text{Be}$  case, one can proceed for several other hypernuclei. Table I gathered the results of the optimization for  $\Lambda$ -hypernucleus up-to Car-

bon hypernucleus. The reaction necessary for the optimal exotic beam production is reported with its target thickness. The selected exotic beam is then mentioned with its optimal kinetic energy and intensity. Finally the yield per second of the hypernucleus of interest is given for a production on 4-centimeter  ${}^{12}\text{C}$  target. Several cases in which a stable beam provide a higher hypernuclear yield can be noted in Table I. Those optimal experimental conditions will be useful for the conceiving the hypernuclear experiments at Super-FRS facility.

#### IV. CONCLUSION

A general procedure was developed in order to determine the optimal experimental conditions for the production of exotic hypernuclei within the Super-FRS fragment separator of the new FAIR facility, in which future hypernuclear spectroscopy experiments will take place. This optimization process includes the theoretical models for the hypernuclear production estimations and for the production of exotic beam from the fragmentation of the primary beam on the production target. It also included Monte Carlo simulations of the beam transportation from the secondary beam production site to the experimental area in which the hypernuclear production and afterwards spectroscopy will take place. The optimization procedure combines those different results and tries to

TABLE I. Summary of all results from the optimization procedure. All  $\Lambda$ -hypernuclei up-to Carbon isotopes were considered, and for each, the optimal experimental conditions are reported: The reaction necessary to produce the exotic beam, the target thickness, the exotic beam selected to produce the hypernuclei of interest on a 4-centimeter  $^{12}\text{C}$  target, the exotic beam kinetic energy and the intensity, and the resulting hypernuclear yield.

	Reaction	Target (cm)	$2^{nd}$ beam	$E_k$ (A GeV)	I ( $10^6/\text{s}$ )	Yield (/s)
$^8_\Lambda\text{C}$	$^{14}\text{N}+^9\text{Be}$	5.5	$^{12}\text{N}$	1.94	5.1	0.2
$^9_\Lambda\text{C}$	$^{14}\text{N}+^9\text{Be}$	5.5	$^{12}\text{N}$	1.94	5.1	0.8
$^{10}_\Lambda\text{C}$	$^{14}\text{N}+^9\text{Be}$	5.5	$^{12}\text{N}$	1.94	5.1	1.5
$^{11}_\Lambda\text{C}$	$^{14}\text{N}+^9\text{Be}$	5.5	$^{12}\text{N}$	1.94	5.1	0.9
$^7_\Lambda\text{B}$	$^{14}\text{N}+^9\text{Be}$	5.5	$^{12}\text{N}$	1.94	5.1	0.7
$^8_\Lambda\text{B}$	$^{14}\text{N}+^9\text{Be}$	5.5	$^{12}\text{N}$	1.94	5.1	2.7
$^9_\Lambda\text{B}$	$^{14}\text{N}+^9\text{Be}$	5.5	$^{12}\text{N}$	1.94	5.1	3.5
$^{10}_\Lambda\text{B}$	$^{14}\text{N}+^9\text{Be}$	5.5	$^{12}\text{N}$	1.94	5.1	2.5
$^{11}_\Lambda\text{B}$	$^{20}\text{Ne}+^9\text{Be}$	2	$^{17}\text{F}$	1.97	5.7	1.2
$^5_\Lambda\text{Be}$	$^{14}\text{N}+^9\text{Be}$	5.5	$^{12}\text{N}$	1.94	5.1	0.6
$^6_\Lambda\text{Be}$	$^{14}\text{N}+^9\text{Be}$	5.5	$^{12}\text{N}$	1.94	5.1	1.9
$^7_\Lambda\text{Be}$	$^{14}\text{N}+^9\text{Be}$	5.5	$^{12}\text{N}$	1.94	5.1	3.9
$^8_\Lambda\text{Be}$	$^{14}\text{N}+^9\text{Be}$	5.5	$^{12}\text{N}$	1.94	5.1	4.0
$^9_\Lambda\text{Be}$	stable beam		$^{16}\text{O}$	2.	10.	4.4
$^{10}_\Lambda\text{Be}$	stable beam		$^{14}\text{N}$	2.	10	3.1
$^{11}_\Lambda\text{Be}$	$^{23}\text{Na}+^{11}\text{B}$	15.5	$^{12}\text{B}$	1.79	1.2	0.6
$^4_\Lambda\text{Li}$	$^{20}\text{Ne}+^9\text{Be}$	2	$^{17}\text{F}$	1.97	5.7	1.1
$^5_\Lambda\text{Li}$	$^{12}\text{C}+^9\text{Be}$	6	$^{10}\text{C}$	1.94	5.1	2.5
$^6_\Lambda\text{Li}$	$^{14}\text{N}+^9\text{Be}$	5.5	$^{12}\text{N}$	1.94	5.1	4.3
$^7_\Lambda\text{Li}$	stable beam		$^{14}\text{N}$	2.	10.	5.2
$^8_\Lambda\text{Li}$	$^{20}\text{Ne}+^9\text{Be}$	2	$^{17}\text{F}$	1.97	5.7	3.7
$^9_\Lambda\text{Li}$	$^{16}\text{O}+^9\text{Be}$	5.5	$^{14}\text{O}$	1.93	5.5	2.2
$^{10}_\Lambda\text{Li}$	$^{23}\text{Na}+^{11}\text{B}$	15.5	$^{12}\text{B}$	1.79	11.5	1.1
$^{11}_\Lambda\text{Li}$	$^{23}\text{Na}+^{11}\text{B}$	15.5	$^{12}\text{B}$	1.79	11.5	0.12
$^3_\Lambda\text{He}$	$^{14}\text{N}+^9\text{Be}$	5.5	$^{12}\text{N}$	1.94	5.1	1.8
$^4_\Lambda\text{He}$	stable beam		$^{14}\text{N}$	2.	10.	4.1
$^5_\Lambda\text{He}$	stable beam		$^{20}\text{Ne}$	2.0	10.	5.2
$^6_\Lambda\text{He}$	stable beam		$^{12}\text{C}$	2.	10.	4.8
$^7_\Lambda\text{He}$	$^{20}\text{Ne}+^9\text{Be}$	2	$^{17}\text{F}$	1.97	5.7	2.9
$^8_\Lambda\text{He}$	$^{20}\text{Ne}+^9\text{Be}$	2	$^{17}\text{F}$	1.97	5.7	1.4
$^9_\Lambda\text{He}$	$^{23}\text{Na}+^{11}\text{B}$	15.5	$^{12}\text{B}$	1.79	11.5	0.8
$^3_\Lambda\text{H}$	stable beam		$^{16}\text{O}$	2.	10.	5.1
$^4_\Lambda\text{H}$	stable beam		$^{20}\text{Ne}$	2.	10	4.5
$^5_\Lambda\text{H}$	stable beam		$^{14}\text{N}$	2.	10.	3.1
$^6_\Lambda\text{H}$	$^{20}\text{Ne}+^9\text{Be}$	2	$^{17}\text{F}$	1.97	5.7	1.5
$^7_\Lambda\text{H}$	$^{20}\text{Ne}+^9\text{Be}$	2	$^{17}\text{F}$	1.97	5.7	0.5
$^8_\Lambda\text{H}$	$^{23}\text{Ne}+^9\text{Be}$	15.5	$^{12}\text{B}$	1.79	11.5	0.3
$^3_\Lambda\text{n}$	$^{20}\text{Ne}+^9\text{Be}$	2	$^{17}\text{F}$	1.97	5.7	2.1
$^4_\Lambda\text{n}$	$^{20}\text{Ne}+^9\text{Be}$	2	$^{17}\text{F}$	1.97	5.7	1.0

provide the best conditions for any hypernucleus that can be considered. Different results from each step and how their combination creates a very large dataset. An optimal search via the maximization of cost functions gives the best experimental requirements. The case of the  $^8_\Lambda\text{Be}$  hypernucleus was considered, and the optimal conditions that were found are to use a secondary beam of  $^{12}\text{N}$  from fragmentation of a  $^{14}\text{N}$  primary beam on a  $^9\text{Be}$  target. On 4-centimeter  $^{12}\text{C}$  target, around  $4.0 \times 10^3$   $^8_\Lambda\text{Be}$  are produced per second. Under those conditions, and considering as in the previous experiments [5], we can expect close to  $345 \times 10^3$  hypernuclei produced per day with an estimated  $^8_\Lambda\text{Be}$  production cross section of  $11 \mu\text{b}$ . Afterward the design of the experimental apparatus from the detector setups and data acquisition will provide the estimated hypernuclear count rate that can be expected within the recorded data. Additionally the cases of all hypernuclei up-to Carbon hypernuclei were optimized and reported. It will be a useful information for further experiments on proton-rich or neutron-rich hypernuclei. Those results were achieved by a particular quasi-convex combination of the variables that were optimized. There are other possibilities to be explored, especially depending of the weight definition in the cost functions. Furthermore the maxi-max criterion was used and different criterion can be also used to tune the weights. Those additional consideration could provide new perspective to the dataset.

## V. ACKNOWLEDGMENTS

This work has been supported by the HypHI project funded by the Helmholtz association as Helmholtz-University Young Investigators Group VH-NG-239 at GSI, and the German Research Foundation (DFG) under contract number SA 1696/1-1 and EU FP7 HadronPhysics-2 SPHERE. This work has also been supported by the co-funded program of the University of Castilla-La Mancha “Ayudas para estancias de investigadores invitados en la UCLM para el ao 2015” and FEDER 2014-2020. A part of this work was carried out on the HIMSTER high performance computing infrastructure provided by the Helmholtz-Institute Mainz. We would like to thank to A. Botvina, H. Geissel, T. Saito and C. Scheidenberger for the involved discussions.

- 
- [1] P. Koch, B. Muller, and J. Rafelski, Phys. Rep. **142** (1986).
  - [2] S. Margetis et al., Annu. Rev. Nucl. Part. Sci. **50** (2000).
  - [3] H. Tamura, Nucl. Phys. A **752** (2005).
  - [4] T. Saito et al., Letter of Intent (2006).
  - [5] C. Rappold et al., Nucl. Phys. A. **913**, 170 (2013).
  - [6] C. Rappold, E. Kim, T. R. Saito, O. Bertini, S. Bianchin, V. Bozkurt, M. Kavatsyuk, Y. Ma, F. Maas, S. Minami, et al. (HypHI Collaboration), Phys. Rev. C **88**, 041001 (2013).
  - [7] C. Rappold et al., Phys. Lett. **B747**, 129 (2015).
  - [8] O. Hashimoto and H. Tamura, Prog. Part. Nucl. Phys. **57**, 564 (2006).
  - [9] H. Geissel et al., Nucl. Instrum. Meth. B **70** (1992).
  - [10] H. Geissel et al., Annu. Rev. Nucl. Part. Sci. (1995).
  - [11] G. Münzenberg et al., Nucl. Instrum. Meth. B **70** (1992).
  - [12] K. Sümmerer and B. B. Blank, Nucl. Phys. A **701** (2002).
  - [13] K. Sümmerer, Phys. Rev. C **86**, 014601 (2012).
  - [14] N. Iwasa et al., Nucl. Instrum. Meth. B **126** (1997).
  - [15] H. Geissel, H. Weick, M. Winkler, G. Münzenberg, V. Chichkine, M. Yavor, T. Aumann, K. Behr, M. Böhmer, A. Brünle, et al., Nucl. Instrum. Meth. B **204**, 71 (2003).
  - [16] M. Winkler, H. Geissel, H. Weick, B. Achenbach, K.-H. Behr, D. Boutin, A. Brünle, M. Gleim, W. Hüller, C. Karagiannis, et al., Nucl. Instrum. Meth. B **266**, 4183 (2008).
  - [17] A. S. Botvina, I. N. Mishustin, and J. Pochodzalla, Phys. Rev. C **86**, 011601 (2012).
  - [18] G. Fäldt and C. Wilkin, Z. Phys. A **357**, 241 (1997).
  - [19] M. Abdel-Bary, S. Abdel-Samad, K.-T. Brinkmann, H. Clement, J. Dietrich, E. Doroshkevich, S. Dshe-muchadse, K. Ehrhardt, A. Erhardt, W. Eyrich, et al., Eur. Phys. J. A **46**, 27 (2010).